

26. CURRENT METHODS FOR PREDICTION AND MINIMIZATION OF

LIFT-INDUCED DRAG AT SUPERSONIC SPEEDS

By Harry W. Carlson and F. Edward McLean
NASA Langley Research Center

SUMMARY

The current state of the art of predicting and minimizing lift-induced drag at supersonic speeds as practiced at the Langley Research Center is reviewed. Numerical methods of implementing the linearized theory for use on high-speed electronic computers are outlined, and applications of the methods to wings, wing-body combinations, and complete configurations are studied. It is concluded that the techniques are generally applicable in the supersonic speed range at least up to a Mach number of 3 for configurations employing slender bodies and thin, moderately cambered wings, as represented by current supersonic-transport designs.

INTRODUCTION

In the past few years, a significant part of the theoretical drag-reduction potential of warped supersonic wings (refs. 1 to 3) has been achieved in wind-tunnel experiments (refs. 4 and 5). Successful application of the theoretical concepts has been due in part to the imposition of experimentally determined restraints on camber surface severity (refs. 4 and 6). Experimental studies (refs. 7 to 9) have also shown the manner in which wing warp may be incorporated into complete airplane configurations so as to preserve and enhance the benefits of the wing design. Another recent development has been the implementation of the theory by numerical methods programed for high-speed computers (refs. 10 to 12). These programs provide a versatile set of tools for rapid estimation and optimization of wing aerodynamic characteristics. The purpose of this paper is to review the nature of the theory and numerical methods of implementation and to discuss the findings of experimental studies regarding the applicability of the methods to wings alone, to wing-body combinations, and to complete configurations.

SYMBOLS

C_D drag coefficient
 ΔC_D incremental drag coefficient due to lift
 C_L lift coefficient

$C_{L,des}$	lift coefficient for which the warped wing surface is designed to produce a minimized drag
$C_{L,opt}$	lift coefficient yielding maximum lift-drag ratio for a theoretically optimum surface
C_m	pitching-moment coefficient about the $0.45\bar{c}$ station
$C_{m,0}$	pitching-moment coefficient at zero lift
C_p	pressure coefficient
C_Y	side-force coefficient
c_r	root chord
\bar{c}	mean aerodynamic chord
$(L/D)_{max}$	maximum lift-drag ratio
M	Mach number
$R_{\bar{c}}$	Reynolds number based on mean aerodynamic chord
w	upwash velocity
x^*	wing shear parameter (see fig. 6)
z	camber-surface ordinate
α	angle of attack

DISCUSSION

Numerical Analysis of Lifting Surfaces

An illustration of the representation of a wing in the numerical analysis is given in figure 1. A simplified analysis may be made for the pair of lifting elements shown at the left of the figure. In generating lift, the forward element of the pair creates a downwash field between trailing tip vortices and an upwash field in the remainder of the Mach cone region. Lift generated by the rearward element depends on its attitude relative to the upwash created by the forward element. Linearized theory provides a solution for the lifting characteristics of an element in the flow field created by one or more forward elements, each generating a given lift. The upwash field at the element is related directly to the lift of the forward element and only indirectly to the angle of attack required for that lift; thus, the case in which the required angle is related to a specified load is termed the direct solution. A complete wing represented as an array of elements is shown at the right of figure 1. This

drawing is schematic; in actual practice, many more elements would be used. In the direct solution, lifting pressures are assigned to each of the elements and the required surface slopes are found. In the inverse solution, the surface slopes are specified and the resulting lifting pressures are found. The inverse solution is more complex but may be handled numerically, provided the calculations are made by following a precise routine - that is, by working from the forward to the rearward elements.

It may be observed that the greatest benefits of warping are derived for wings with leading edges swept behind the Mach line. The leading-edge elements, acting in the upwash field of the forward elements, generate fairly large amounts of lift on a forward-facing slope, and thus produce a thrust component rather than a drag component. However, even for planforms for which the drag reduction is small, the use of twist and camber is worthy of investigation, since it can help reduce the problem of the supersonic aerodynamic-center shift.

Figures 2 and 3 illustrate the design and analysis tools provided by the numerical solutions of the theory. An example of the direct problem is shown in figure 2. A planform and a desired loading distribution (represented by the arrows) are specified, and a surface which will support that loading is determined. Symbols on the plot represent wing forces, and inset sketches show the corresponding shapes of the camber surfaces as determined by use of the method of reference 10. The circular symbol represents a solution for the surface required to yield an arbitrarily selected distribution of load at a specified lift coefficient. The somewhat unusual loading distribution selected is only one of many possible distributions.

By determining the solutions for three or more specific load distributions and by using a numerical evaluation of the mutual interference of loadings and surfaces, an optimum combination of loadings for minimum drag is obtained. The square symbol represents the solution for a surface defined by an optimum combination of three loadings. The solid line shows the variation of drag increment with lift for a wing which is allowed to assume the optimum shape at all lift coefficients. Since a real wing must have a fixed surface shape, this curve forms a lower-bound envelope of possible drag reduction for a given planform.

Because of necessary departures from the idealized optimum camber surfaces in airplane design, it is advantageous to have a means of evaluating arbitrarily selected shapes for use in trade studies. In figure 3 is shown an example of the inverse problem treated in references 11 and 12. A planform and a cambered surface shape are given, and the lift loading and the resultant forces are determined. The circular symbol represents the machine solution for a wing of specified shape at a reference attitude of 0° , and the corresponding inset sketch shows the distribution of lifting pressures. A special case of camber surface shape is a flat plate. The solution for the lifting pressures and forces on a flat wing having the same planform as the wing of specified shape is represented by the dashed line. These two solutions may be combined to define the pressures and drag for the cambered wing of specified shape as the angle of attack and lift coefficient are varied. The solid line represents

the combined solution and the inset sketches along this line illustrate the variations in wing loading with lift coefficient.

The computer programs thus serve the following purposes:

(1) To define a lower bound of possible drag reduction and describe the theoretical lower-bound shapes

(2) To define the loadings and lift-drag characteristics of arbitrarily selected wing shapes

(3) To describe the loadings and lift-drag characteristics of flat wings having the same planform as the wings of specified shape, the lift-drag characteristics being a base point for judging the benefits of twist and camber

In current configuration analyses, the lifting effects for an infinitely thin wing calculated by use of these programs are added directly to the effects of thickness evaluated independently by use of machine programs based on supersonic-area-rule concepts (ref. 13). Thus, the possibility of mutual interaction between lift and volume is not considered. In addition, no account is taken of the leading-edge suction forces which, although important at subsonic speeds, have not been found to exist to any appreciable extent at supersonic speeds. The presence of a detached leading-edge vortex flow, which could influence to some degree the loadings and forces at supersonic speeds, is similarly neglected.

Application of Analysis Methods

Application to wings alone.- An example of the use of wing warp to provide a reduction in drag at lifting conditions and an improvement in trim characteristics is shown in figure 4. An investigation of the semispan wing shown at the upper left of the figure was conducted at a Mach number of about 2 and a Reynolds number of 4.4×10^6 in the Langley 4- by 4-foot supersonic pressure tunnel (ref. 4). A warped wing and a flat wing of the same planform were investigated. The experimental results are compared with theoretical curves for these two wings and with a theoretical curve for a wing defined by an optimum combination of loadings. The drag of the warped wing is somewhat higher than that of the flat wing at zero lift, but is significantly lower than that of the flat wing at the higher lift coefficients. The fact that the experimental results fail to achieve the theoretical drag levels for the optimum surface is to be expected, inasmuch as an infinite incidence at the root chord is unrealistically assumed for the theoretically optimum surface. Although the optimum loading theory indicates a maximum lift-drag ratio for a lift coefficient of about 0.16, it was found that a wing designed for a theoretically minimum drag at that lift coefficient actually performed little better than the flat wing. Experimental evidence has shown that better results are obtained when the lift for maximum lift-drag ratio is due in part to the warped surface and in part to the angle of attack of that surface. The particular warped wing surface shown in this figure was designed to produce a lift coefficient of 0.08. In addition, the wing employed restrictions in incidence of the root chord and in

local loading (ref. 6). The inverse program may be used to assure that these departures from the theoretically optimum surface introduce no large penalties. Figure 4 also shows that, in addition to providing for reduced drag, the wing warping results in a more positive pitching-moment coefficient which permits more efficient trimming of the configuration.

The necessity for realistic restraints on the severity of camber surfaces is illustrated in figure 5. Measured and predicted maximum lift-drag ratio and pitching-moment coefficient at zero lift are shown for a series of three wings (from ref. 4) differing only in the degree of warping, which is dictated by the design lift coefficient. The design lift coefficient $C_{L,des}$ is referred to the lift coefficient giving maximum lift-drag ratio for the theoretically optimum wing surface $C_{L,opt}$. Inset sketches show the increasing severity of the wing surface with increases in the design lift coefficient. The highest lift-drag ratio obtained experimentally is lower than the theoretical maximum and occurs for a value of $C_{L,des}$ about half as large as that required for the theoretical maximum. This result is probably due to the increasing inapplicability of the linearized theory as the surface becomes more highly warped. It should not be assumed that a ratio of $C_{L,des}$ to $C_{L,opt}$ of 0.5 is to be used in all instances. The choice of design lift coefficient will be influenced by the planform and the Mach number and by moment considerations as well. It should be noted that, as shown at the right of the figure, the beneficial pitching-moment coefficient at zero lift increases steadily as the value of $C_{L,des}/C_{L,opt}$ is increased from 0 to 1.0.

The linearized theory, on which the methods of twisted and cambered wing design are based, sets specific requirements for the surface slope with respect to the flight direction but imposes no restrictions on the slope with respect to the lateral direction. Results from a recent experimental investigation which illustrate the importance of lateral-slope considerations are shown in figure 6. The models were variations of the basic wing shown in figure 4, which had a design lift coefficient of 0.08. The wings have been sheared to produce a flat lateral section at various stations x^* along the root chord of the wing, as shown in the inset sketch at the upper right. The variation of measured $(L/D)_{max}$ with the shear parameter x^*/c_r is shown, along with sketches of the side views of the semispan wings. The experimental data indicate that maximum performance is attained for values of x^*/c_r near 0.5. It would appear that best results are obtained when the surface is arranged to lie in as nearly a single plane as possible without changing the streamwise slopes. The results of an experimental study in which wing dihedral is the variable (ref. 14) lead to a similar conclusion.

Application to wing-bodies.- An important consideration in the application of twisted and cambered wing design is the manner in which wing and fuselage are combined. Reference 7 gives maximum lift-drag ratios for wing-fuselage combinations employing the basic cambered wing of figure 4, and these data are presented in figure 7. Also, for reference purposes, data are presented for a combination in which the uncambered or flat wing is used. It was previously believed that a fuselage aligned with the free stream would be beneficial in

that it would cover up the troublesome inboard wing region having large surface slopes. Experimental data for the first of the warped-wing—fuselage configurations in figure 7 indicate, however, that the combination with a fuselage so alined has a maximum lift-drag ratio only slightly larger than that of the flat-wing—body configuration. Another possible way of combining the wing and fuselage is to aline the fuselage with the wing root chord. As shown in figure 7, the maximum lift-drag ratio for this combination is considerably larger than that for the flat-wing—body configuration. The final configuration in this figure employs a fuselage which is alined with the root chord but which has a reflex at the wing apex and at the root-chord trailing edge. In effect, the thickness of this configuration, both wing and fuselage, is displaced symmetrically about the camber surface defined for the wing planform. For the design condition of $C_L = 0.08$ the fuselage ahead of and behind the wing surface is alined with the free stream and carries little or no lift. This wing-body combination produced the highest maximum lift-drag ratio of the test configurations; the ratio was about 1.1 larger than for the uncambered- or flat-wing—body configuration. It would appear that such an arrangement of the configuration volume preserves the distribution of wing loading prescribed by the wing theory. Theoretical maximum lift-drag ratios evaluated by use of the mean-camber-surface concept, which is discussed in the following paragraph, predict reasonably well the performance gains of the last two configurations in figure 7 but fail to assess properly the penalties associated with the streamwise fuselage alinement.

The concept of a mean camber surface is quite useful in analyzing the characteristics of a wing-body configuration with appreciable thickness. An application of this kind of analysis to the prediction of interference effects for a delta-wing—wedge-body model at $M = 2.0$ (ref. 15) is shown in figure 8. Lift-drag polars and curves for angle of attack as a function of lift coefficient are shown for a high-wing and a low-wing configuration. The lift characteristics have been estimated from program calculations for a warped surface formed by the locus of points midway between the upper and lower model surfaces. Since the numerical solution cannot work with discontinuous slopes, it is necessary in this example to approximate the mean camber surface with a surface that varies gradually from element to element. The step in the surface is thus replaced by a series of ramps extending over a number of grid elements. It is also necessary to tax the machine storage capacity in order to obtain a good approximation of this model surface, obviously an extreme case of a warped wing surface. The data show that the high-wing configuration has lower drag at lifting condition than does the low-wing configuration and that the theory correctly predicts this drag. It should be noted that the mean camber surface used to represent the high-wing model more nearly corresponds to the surface required for an optimum combination of loads. The use of favorable-interference concepts, as exemplified by the high-wing model, is in a sense a special case of twist and camber. As shown at the right of the figure, the theory somewhat overestimates the influence of the wedge in the generation of interference lift, perhaps because in real flow the body pressure field extends some distance ahead of the theoretically sonic leading-edge wing.

Since a mean camber surface may be used to represent the lifting effects of a wing-body combination, it would be expected that, conversely, lifting

effects for a theoretically determined mean camber surface would be best retained with a symmetrical distribution of thickness above and below that surface.

Positioning of engine nacelles or stores has an important influence on configuration aerodynamic characteristics. Fairly large variations in wave drag at zero lift can result from variations of nacelle location relative to the wing-fuselage. As illustrated in figure 9, nacelle alinement also influences the drag. This figure presents data from reference 8 and shows the variation of ΔC_D for the wing-nacelle combination with alinement or cant angle at $C_L = 0.16$. By definition, the drag increment is zero for zero cant angle. As shown in the inset sketch, a nacelle-pylon installation experiences a side force due to the flow angularity produced by the wing. A component of this force acts in the drag direction. When the nacelle is alined with the local flow, there is no side force and no drag component. When the nacelle is alined with the airplane axis or the free stream, there is a side force normal to the nacelle but the drag component is zero. For a cant angle larger than the flow angle, the side-force vector reverses and considerable drag can result. Also, for negative cant angles, the drag penalties can become large. It is interesting to note that a thrust, not a drag, is indicated for cant angles between the free stream and the local flow, with the maximum thrust halfway between the two. Setting a nacelle-pylon combination at such an angle results in somewhat higher drag at zero lift but produces, as does a twisted or cambered wing, a reduction in drag at design conditions. Calculations of local-flow angle is not now a part of the machine programs, but may be handled by a graphical integration of pressures to obtain velocity potential and a subsequent differentiation to obtain surface velocities. When calculated surface angles are used to optimize nacelle-pylon alinement, some correction should be made for the tendency to overestimate flow angularity off the wing surface at the pylon location. In the example given here the measured flow angle at the nacelle was only about two-thirds of the predicted surface angles. These considerations are also applicable to any vertical surfaces displaced from the airplane axis (e.g., outboard vertical fins). This rather simplified analysis of a complex situation has proved effective in obtaining drag reduction.

Application to complete configurations.- The individual elements of design philosophy as applied to airplane components have been discussed. In this section of the paper the integration of these elements into complete-configuration design is considered. The supersonic-transport design of reference 9 shown in figure 10 has been derived in part from skin-friction and wave-drag considerations which tend to minimize drag at zero lift. It also employs to some degree all the design considerations previously discussed - that is, the restricted design lift coefficient for the wing surface, the shear consideration, the nacelle and fin alinement, and the symmetrical distribution of thickness about the wing camber plane. In addition, for that region of the wing influenced by the nacelle thickness pressures (the shaded area and the lower cross section) the computed wing surface has been altered in order that the net lift distribution on the wing surface including the nacelle-induced pressures would be the same as that specified by the wing theory. The wing loading due to the nacelle pressure field has been calculated and the wing mean camber surface has been

reflexed to introduce a compensating loading. Detailed interference considerations discussed in reference 16 lead to the same design procedure.

Shown in figure 11 are the lift-drag characteristics of the optimized configuration at a Mach number of 2.6 for a tunnel Reynolds number of 4.5×10^6 . Data on the left side of the figure are for the wing-fuselage combinations alone. Measured and calculated lift-drag polars are plotted for the warped-wing-body and for a similar configuration without wing warp. For the higher lift coefficients considered, the warped-wing-body is seen to provide a significant reduction in drag. On the right side of the figure, the lift-drag polar for the complete configuration shows the effect of the nacelles and vertical fins added in accordance with the previously outlined design concepts. Although there is a sizable increase of drag at zero lift, favorable-interference considerations and wing reflex have nearly compensated for the additional nacelle and fin wave drag and skin-friction drag for practical values of lift coefficient. Furthermore, the tunnel $(L/D)_{\max}$ of 7.9 is for a complete configuration which has substantial pitching moment at zero lift and which would be expected to have little or no trim drag penalty. Extrapolation to full-scale cruise flight conditions yields a value of $(L/D)_{\max}$ of about 9.5.

The benefits of the wing twist and camber and favorable-interference considerations are not confined to a specific design point, but have been found to extend over wide ranges of Mach number and lift coefficient, as shown in references 9 and 17.

CONCLUDING REMARKS

The design and estimation techniques discussed herein have been shown to be applicable in the supersonic range at least up to a Mach number of 3.0 for configurations employing slender bodies and thin, moderately cambered wings. Thus, if a configuration meets the requirements for efficient supersonic cruise (a necessity for supersonic-transport designs), the methods may be used with some confidence in estimating and optimizing the aerodynamic characteristics. With configurations for which supersonic cruise efficiency is not a major consideration (e.g., supersonic dash vehicles), there may be some question as to the applicability of methods based on linearized theory.

REFERENCES

1. Jones, Robert T.: Theoretical Determination of the Minimum Drag of Airfoils at Supersonic Speeds. *J. Aeron. Sci.*, vol. 19, no. 12, Dec. 1952, pp. 813-822.
2. Grant, Frederick C.: The Proper Combination of Lift Loadings for Least Drag on a Supersonic Wing. NACA Rept. 1275, 1956. (Supersedes NACA TN 3533.)
3. Brown, Clinton E.; and McLean, Francis E.: The Problem of Obtaining High Lift-Drag Ratios at Supersonic Speeds. *J. Aero/Space Sci.*, vol. 26, no. 5, May 1959, pp. 298-302.
4. Carlson, Harry W.: Aerodynamic Characteristics at Mach Number 2.05 of a Series of Highly Swept Arrow Wings Employing Various Degrees of Twist and Camber. NASA TM X-332, 1960.
5. McLean, F. Edward; and Fuller, Dennis E.: Effects of Thickness on Supersonic Performance of a Wing-Body Configuration Employing a Warped Highly Swept Arrow Wing. NASA TN D-3034, 1965.
6. Brown, Clinton E.; McLean, F. E.; and Klunker, E. B.: Theoretical and Experimental Studies of Cambered and Twisted Wings Optimized for Flight at Supersonic Speeds. *Advan. in Aeron. Sci.*, vol. 3, Pergamon Press, 1961, pp. 415-431.
7. Carlson, Harry W.: Longitudinal Aerodynamic Characteristics at Mach Number 2.02 of a Series of Wing-Body Configurations Employing a Cambered and Twisted Arrow Wing. NASA TM X-838, 1963.
8. Landrum, Emma Jean: Effect of Nacelle Orientation on the Aerodynamic Characteristics of an Arrow Wing-Body Configuration at Mach Number 2.03. NASA TN D-3284, 1966.
9. Morris, Odell A.; and Fournier, Roger H.: Aerodynamic Characteristics at Mach Numbers 2.30, 2.60, and 2.96 of a Supersonic Transport Model Having a Fixed, Warped Wing. NASA TM X-1115, 1965.
10. Carlson, Harry W.; and Middleton, Wilbur D.: A Numerical Method for the Design of Camber Surfaces of Supersonic Wings With Arbitrary Planforms. NASA TN D-2341, 1964.
11. Middleton, Wilbur D.; and Carlson, Harry W.: A Numerical Method for Calculating the Flat-Plate Pressure Distributions on Supersonic Wings of Arbitrary Planform. NASA TN D-2570, 1965.
12. Middleton, Wilbur D.; and Carlson, Harry W.: Numerical Method of Estimating and Optimizing Supersonic Aerodynamic Characteristics of Arbitrary Planform Wings. *J. Aircraft*, vol. 2, no. 4, July-Aug. 1965, pp. 261-265.

13. Harris, Roy V., Jr.: An Analysis and Correlation of Aircraft Wave Drag. NASA TM X-947, 1964.
14. Middleton, Wilbur D.; and Carlson, Harry W.: Supersonic Longitudinal Aerodynamic Characteristics of Two Wing-Body Configurations Employing Warped Arrow Wings of Varying Dihedral. NASA TM X-897, 1963.
15. Morris, Odell A.: Aerodynamic Characteristics in Pitch at a Mach Number of 2.01 of Several Wing-Body Combinations With Wedge-Shaped Bodies Located Above and Below a 54.5° Swept Delta Wing. NASA TN D-1823, 1963.
16. Robins, A. Warner; Morris, Odell A.; and Harris, Roy V., Jr.: Recent Research Results in the Aerodynamics of Supersonic Vehicles. Paper No. 65-717, Am. Inst. Aeron. Astronaut., Nov. 1965.
17. Middleton, Wilbur D.; and Sorrells, Russell B.: Off-Design Aerodynamic Characteristics at Mach Numbers 1.61 and 2.20 of a Series of Highly Swept Arrow Wings Designed for Mach Number 2.0 Employing Various Degrees of Twist and Camber. NASA TN D-1630, 1963.

LIFTING-SURFACE REPRESENTATION

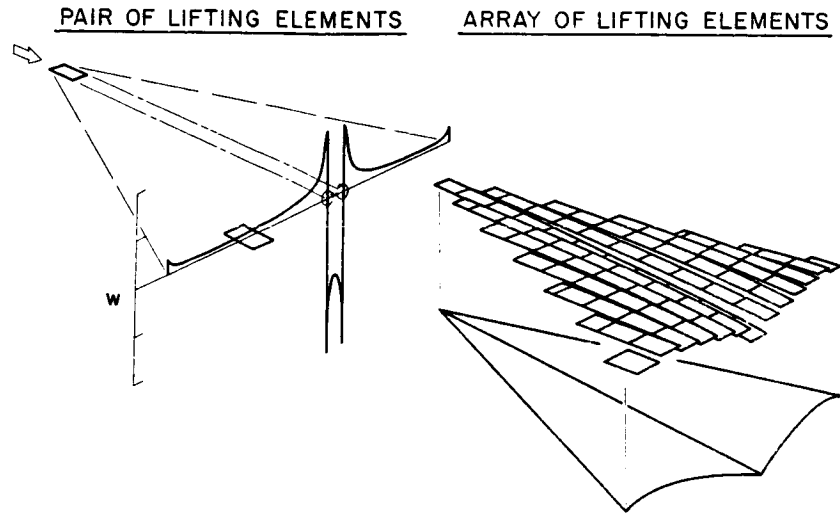


Figure 1

DESIGN METHODS

WING SHAPE AND CORRESPONDING DRAG FOR SPECIFIED LOADING

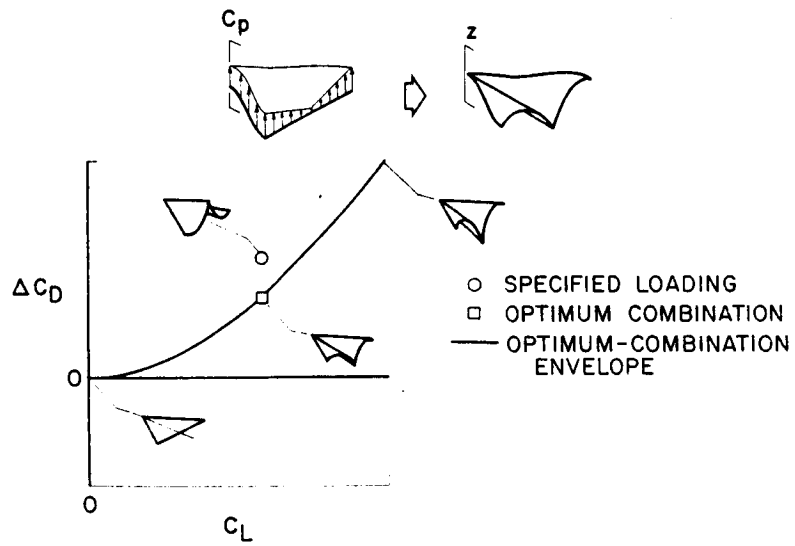


Figure 2

ESTIMATION METHODS

LOADING AND CORRESPONDING DRAG FOR SPECIFIED SHAPE

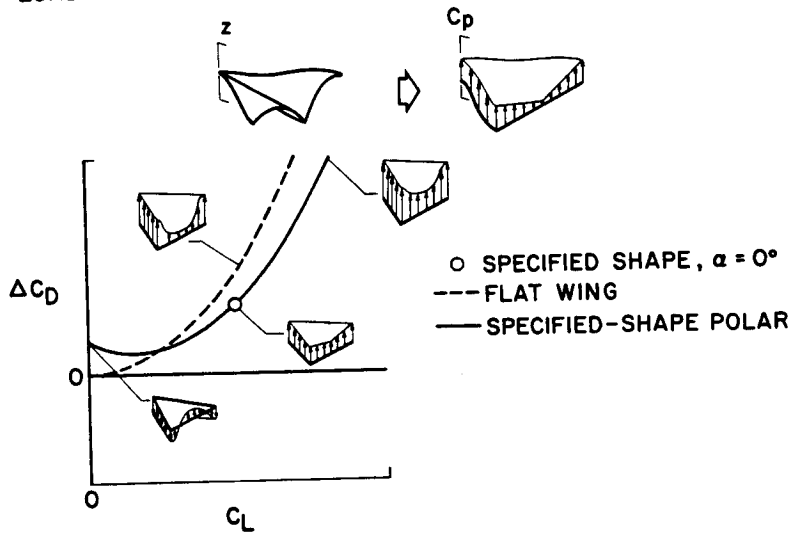


Figure 3

AN EXAMPLE OF THE USE OF WING WARP

M=2

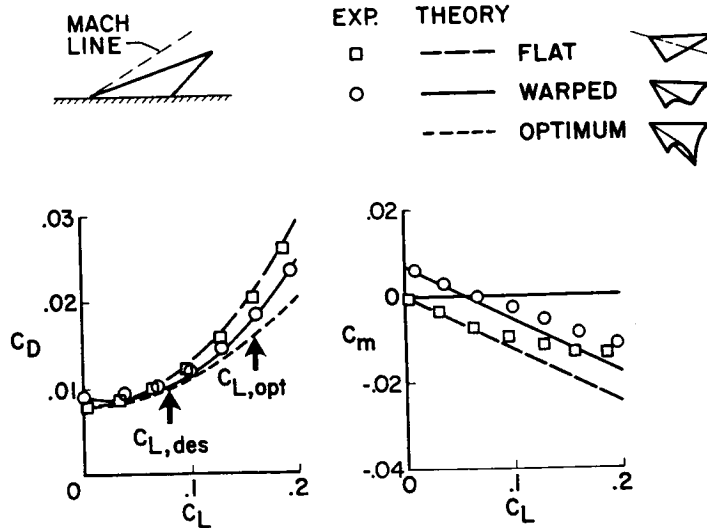


Figure 4

EFFECT OF DESIGN LIFT COEFFICIENT

M=2

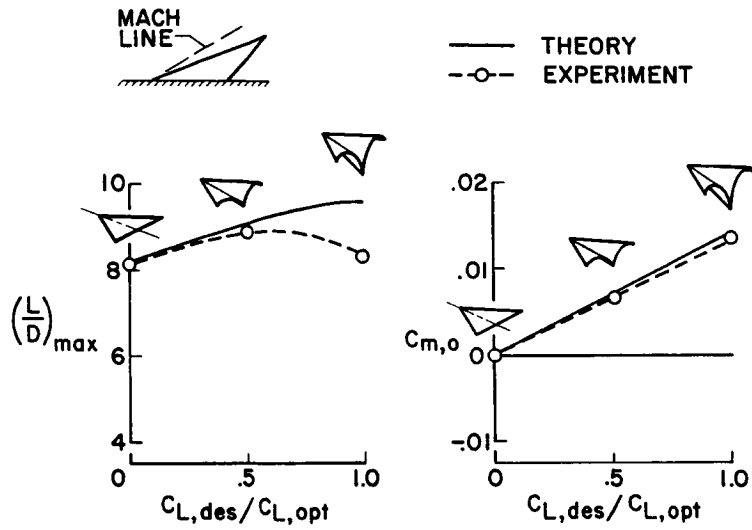


Figure 5

EFFECT OF WING SHEAR EXPERIMENT; M=2

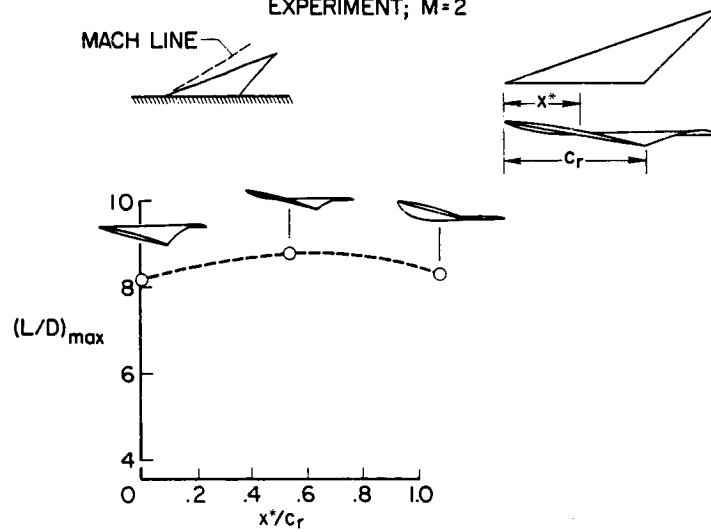


Figure 6

EFFECT OF FUSELAGE ALINEMENT

M=2

EXPERIMENT
THEORY

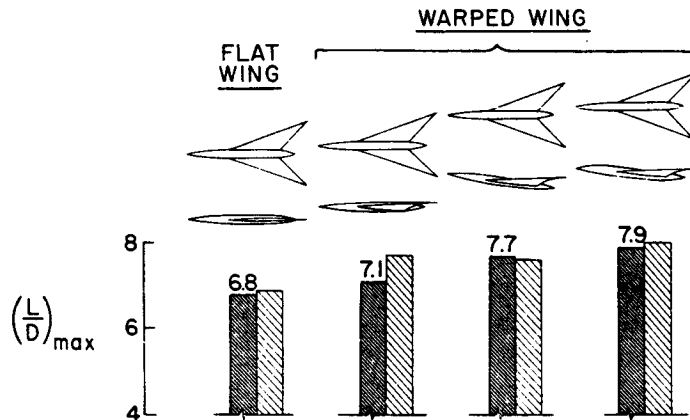


Figure 7

CONCEPT OF MEAN CAMBER SURFACE

M = 2

EXP. THEORY

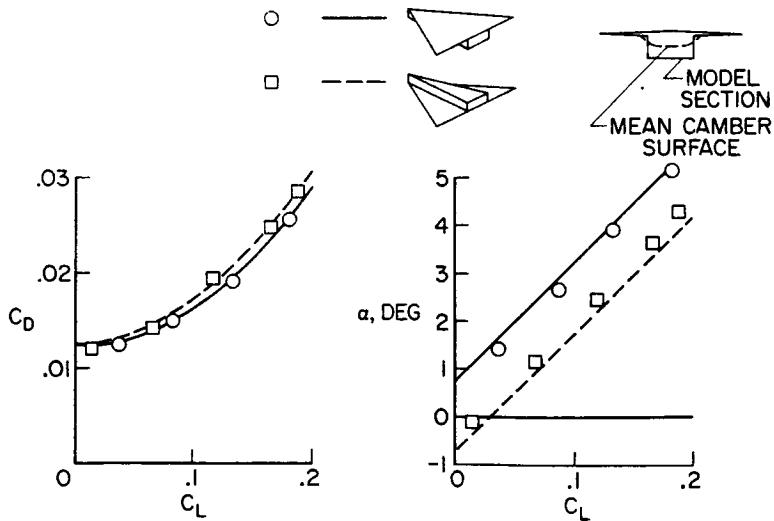


Figure 8

EFFECT OF NACELLE ALINEMENT

$M=2; C_L=0.16$

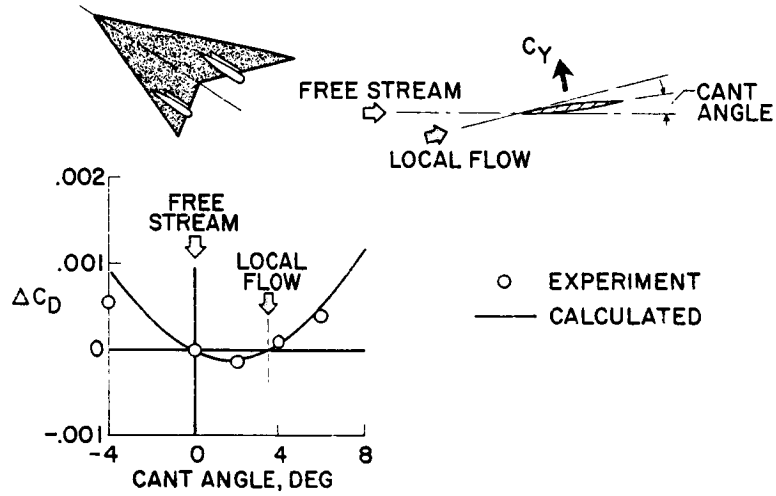


Figure 9

A CONFIGURATION EMPLOYING OPTIMIZED LIFT DESIGN FEATURES

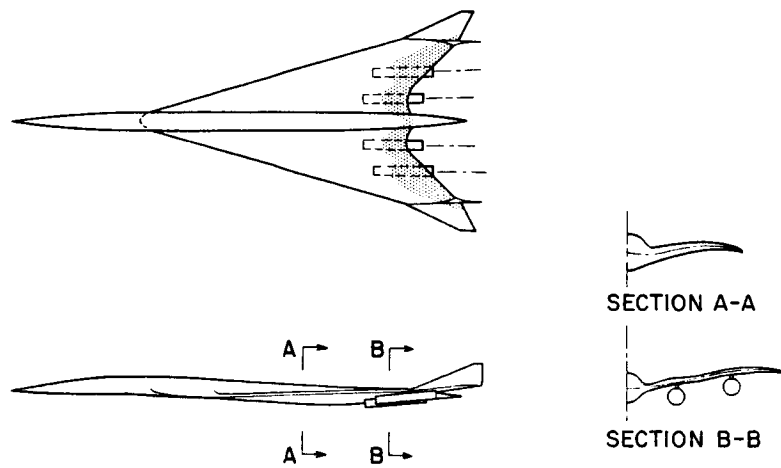


Figure 10

LIFT AND DRAG OF OPTIMIZED CONFIGURATION

$M=2.6; R_{\bar{c}}=4.5 \times 10^6$

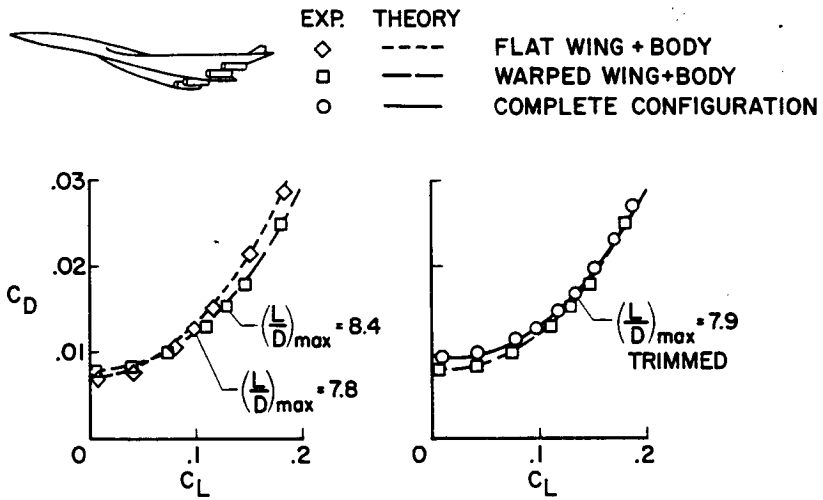


Figure 11